

www.acsami.org Research Article

Thermodynamic Interactions as a Descriptor of Cross-Over in Nonaqueous Redox Flow Battery Membranes

Patrick M. McCormack, Gary M. Koenig, Jr.,* and Geoffrey M. Geise*



Cite This: ACS Appl. Mater. Interfaces 2021, 13, 49331-49339



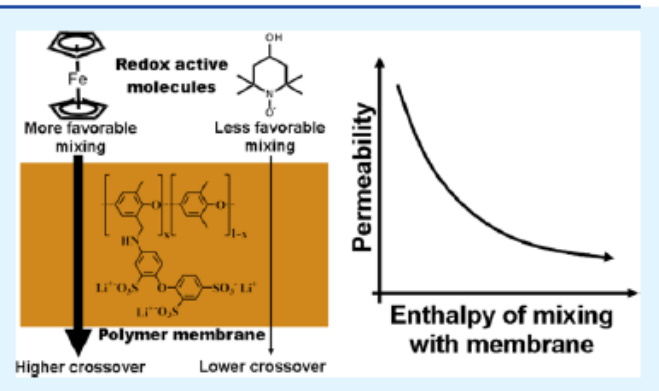
ACCESS I

Metrics & More

Article Recommendations

Supporting Information

ABSTRACT: Grid-scale energy storage is increasingly needed as wind, solar, and other intermittent renewable energy sources become more prevalent. Redox flow batteries (RFBs) are well suited to this application because of the advantages in scalability and modularity over competing technologies. Commercial aqueous flow batteries often have low energy density, but nonaqueous RFBs can offer higher energy density. Nonaqueous RFBs have not been studied as extensively as aqueous RFBs, and the use of organic solvents and organic active materials in nonaqueous RFBs presents unique membrane separator challenges compared to aqueous systems. Specifically, organic active material cross-over, which degrades battery performance, may be affected by membrane/active material thermodynamic interactions in a fundamentally



different way than ionic active material cross-over in aqueous RFB membranes. Hansen solubility parameters (HSPs) were used to quantify these interactions and explain differences in organic active material permeability properties. Probe molecules with a more unfavorable HSP-determined enthalpy of mixing with the membrane polymer exhibited lower permeability or cross-over properties. The HSP approach, which accounts for the uncharged polymer backbone and the charged side chain, revealed that interactions between the uncharged organic probe molecule and the hydrophobic polymer backbone were more important for determining permeability or cross-over properties than interactions between the probe molecule and the hydrophilic side chain. This result is significant for nonaqueous RFBs because it suggests a decoupling of ionic conduction expected to predominantly occur in charged polymer regions and cross-over of organic molecules via hydrophobic or uncharged polymer regions. Such decoupling is not expected in aqueous systems where active materials are often polar or ionic and both cross-over and conduction occur predominantly in charged polymer regions. For nonaqueous RFBs, or other membrane applications where selective organic molecule transport is important, HSP analysis can guide the co-design of the polymer separator materials and soluble organic molecules.

KEYWORDS: nonaqueous flow battery, lithium conducting membrane, separator, functional polymer, energy storage

INTRODUCTION

Redox flow batteries (RFBs) are being developed to address the growing need for grid-scale energy storage. ^{1–5} Generally, these batteries store energy in redox-active molecules that are dissolved in an electrolyte solution. This electrolyte is stored in large tanks and pumped through an electrode stack during electrochemical charge and discharge. This separation of battery capacity (adjustable by the size or number of storage tanks) and power density (adjustable by the size or number of electrode stacks) affords RFBs advantages with regards to modularity and scalability over conventional static batteries. Furthermore, the separation of energy and power has inherent safety advantages because the majority of the reactive species are stored, at any given time, in physically separated tanks. ^{7,8}

The most common commercially available RFB systems are based on vanadium or zinc-bromine chemistry, and both use aqueous electrolytes.⁵ The maximum operating voltage of aqueous RFBs is limited by undesired water splitting side reactions, and this restriction limits the energy density of aqueous RFBs. Nonaqueous RFBs could circumvent this issue and are being developed to improve battery energy density by widening the electrochemical stability window of the electrolyte. ^{9,10} Switching to a nonaqueous solvent also enables the use of new types of redox-active molecules that are unstable or insoluble in aqueous electrolytes. ^{9,11,12}

The anolyte and catholyte solutions (i.e., the two sides) in a RFB power stack must be separated, typically via a membrane. ^{1,3} This membrane separator is a critical battery component because it must facilitate ionic conduction between

Received: August 4, 2021 Accepted: September 23, 2021 Published: October 5, 2021





the anode and cathode while preventing cross-over and subsequent reaction of the soluble redox-active molecules. Membranes have been evaluated and developed for use in the more mature aqueous RFBs, including commercial systems, ^{13–15} but few studies have considered membranes for use in nonaqueous RFBs. ^{10,16}

Battery separator membranes can be porous or nonporous in nature. Many aqueous flow battery systems use nonporous ionexchange membrane (IEM) separators¹⁷ that are similar to the membranes used in fuel cells. Some battery applications, however, use porous membrane separators. 17 In porous membrane separators, a pore network filled with the electrolyte provides pathways for ionic conduction, and ionic conductivity is typically scaled, relative to the bulk electrolyte conductivity, by the porosity and tortuosity of the separator. Porous membranes can be described using a pore flow model, where penetrant molecule transport is modeled as diffusion and/or convection through a tortuous porous network.¹⁸ Membrane permeability and selectivity in porous separators are dictated primarily by the relative sizes of the pores and the penetrant molecules and the relative fraction of the membrane filled with the electrolyte. This approach to obtain a selectively permeable membrane is commonly used in porous separators for both aqueous and nonaqueous batteries. 19-21 Commercially available porous separators, such as Celgard or Daramic, are also sometimes used as separators when testing new redox-active materials.²²⁻²⁴ The pore dimensions in these commercially available separators are very large relative to the size of the molecules, so they promote high conductivity but also result in higher active material permeability or cross-over. 16,17

The transport mechanism is different for porous and nonporous membrane separators. ^{25,26} In nonporous IEMs, transport is often described by the solution-diffusion model where the penetrant molecule first dissolves in the polymer matrix and subsequently diffuses through the solvated membrane before desorbing at the downstream side. 18,25,27 The sorption process in these materials is fundamentally different than the pore partitioning process in porous separators, and the permeability depends on both thermodynamic (sorption) and kinetic (diffusion) factors. The sorption and diffusion processes are affected by a variety of factors, but differences in the permeability of charged molecules are often explained using charge-based exclusion (e.g., Donnan exclusion²⁸) and/or free volume-based mechanisms.²⁹ This solution-diffusion approach is commonly used to describe transport in nonporous materials for other selectively permeable membrane applications including reverse osmosis (RO) and gas separations. 26,27,29,30

The ionic conductivity of polymer membranes has been previously investigated using nonaqueous solvents, in part due to the historical development of the polymer and gel electrolytes. Additionally, conductivity properties of IEMs, developed both for aqueous and nonaqueous applications, have been investigated using nonaqueous electrolytes. The permeability of redox-active molecules through IEMs, a critical metric for quantitatively assessing cross-over, is less understood in nonaqueous solvents. The structure—property tradeoffs between permeability and conductivity in nonaqueous systems are even less developed. This lack of fundamental knowledge is further complicated because nonaqueous flow batteries use a wide range of solvents and redox-active materials. Pala Robust structure—property relationships are needed to inform the permeability of membrane

materials considered for use in the vast space of solvents and redox-active materials of interest for nonaqueous RFBs.

Size-exclusion or free volume effects may influence diffusion strongly enough to explain the permeability differences of some uncharged materials in polymeric membranes, but they may be insufficient for other molecules, including moderately hydrophobic solute molecules, where other thermodynamic effects may be more significant. ^{36,37} In these cases, thermodynamic interactions (e.g., hydrophobic—hydrophobic interactions between the solute and uncharged polymer) may also significantly affect permeability properties because of the sorption contribution to permeability.

For example, for the rejection of a series of hydrophilic molecules of varying size through a RO membrane, rejection was reported to increase (i.e., permeability decreased) with increased molecule size, as predicted by size-exclusion or free volume approaches.³⁶ However, hydrophobic interactions cause moderately hydrophobic molecules to sorb into the polymer matrix to a greater extent than hydrophilic materials. This situation can result in some larger hydrophobic molecules permeating faster than smaller hydrophilic molecules and can create rejection trends that do not correlate well with molecule size.36 Such a situation illustrates the importance of considering thermodynamic interactions in addition to sizebased approaches commonly used to describe diffusion. These thermodynamic interactions are likely to be more important in nonaqueous RFB membranes because the redox molecules for nonaqueous RFBs are typically more hydrophobic compared to the ionic or hydrophilic organic molecules used in aqueous RFBs.10

Our previous work investigating ion-conductive and -selective membranes further suggested that thermodynamic interactions were significant in nonaqueous flow battery membranes. Increasing the charge density of an ion-exchange membrane did not noticeably influence the permeability of ferrocene, a nonpolar molecule, even though both solvent uptake and ionic conductivity increased. It was hypothesized that this result stemmed from stronger interactions between ferrocene and the hydrophobic polymer backbone compared to interactions between ferrocene and the hydrophilic charged side chains.

Here, the hypothesized influence of thermodynamic interactions in our previously reported membrane material was studied in further detail by investigating the permeability of a series of organic probe molecules, which included redoxactive molecules, through a polymeric cation-exchange membrane. In general, organic probe molecules that more favorably interact with the polymer backbone tended to permeate through the membrane more rapidly compared to molecules that interact less favorably with the membrane. These structure—property relationships can be explained using a regular solution theory (Hansen solubility parameter) framework that could be generalized to other systems and could guide polymer membrane material design for non-aqueous RFB applications or other membrane applications where organic molecule transport is important.

■ THEORY

A solubility prediction approach was used to quantify and analyze the thermodynamic interactions that influence redoxactive or probe molecule permeability. The rationale for this approach was based on the role that thermodynamic solubility or partitioning plays in determining permeability in dense nonporous polymers. 25,27 Using regular solution theory, the Gibbs free energy of mixing can be described in terms of an ideal entropy of mixing and a nonideal enthalpy of mixing.³⁸ Solubility parameter approaches apply this theory to describe and predict solubility, or the favorability of mixing, by using empirical methods to estimate the enthalpy of mixing and the magnitude of the excess enthalpy that causes a solute to become insoluble in a solvent. This theoretical basis for solubility parameters has been leveraged to describe gas permeability in membranes, pervaporation membrane selectivity, and solute rejection in organic solvent nanofiltration. 39-42

The Hildebrand solubility parameter, δ , was developed first.³⁸ It is defined as the square root of the cohesive energy density, which is the total potential energy contained in a liquid that results from the intermolecular forces between molecules. The Hildebrand solubility parameter is based on the premise that a solute and solvent with more similar cohesive energy densities will minimize the magnitude of an unfavorable excess enthalpy. Specifically, the theory suggests that the difference of the solute and the solvent solubility parameters is proportional to the enthalpy of mixing (or excess enthalpy). A smaller positive excess enthalpy corresponds to a higher probability of solute solubility in the solvent, or in the context of this study, higher cross-over through the RFB membrane separator. Hildebrand's approach, however, combines all of the enthalpic effects into a single parameter, and this can lead to inaccurate predictions, especially for polar molecules or other systems with more complicated inter-

The Hansen solubility parameter (HSP) improved on Hildebrand's method by splitting the cohesive energy density into component parts associated with different types of intermolecular interactions: dispersive interactions (δD), dipole interactions (δP), and hydrogen bonding interactions (δH) . This approach can improve solubility predictions in both polar and nonpolar systems. Instead of the simple difference of solubility parameters, the HSP method defines a distance, Ra, that depends on the three HSP components of both the solute and solvent

$$R_{a} = \sqrt{4(\delta D_{1} - \delta D_{2})^{2} + (\delta P_{1} - \delta P_{2})^{2} + (\delta H_{1} - \delta H_{2})^{2}}$$
(1)

The factor of 4 in the dispersive energy term was empirically added to improve predictions.⁴⁵ As with the Hildebrand solubility parameter, a smaller distance, R2, indicates that the two molecules are predicted to have a smaller enthalpy of mixing (i.e., the interactions are closer to ideal). The HSP method also introduces a solute- and concentration-dependent cutoff distance, R_0 . If R_2 is less than R_0 , the solute is predicted to be soluble in the solvent at the concentration at which R_0 was defined. A sphere analogy is useful due to the similarity of eq 1 to the distance between two points in 3-D space, and the cutoff distance is typically referred to as a radius. Therefore, a solute has three HSP components and a radius, and solvents with HSP components that lie within the sphere defined by the solute HSP components and radius are predicted to be good solvents for the solute.

As with all solubility parameters, Hansen's method contains assumptions, and the method does not necessarily account for everything that determines solubility. The method was originally developed for paints and polymers, and many of the assumptions were made to reflect these use cases. The

result is that small-molecule solubility is less accurately predicted with Hansen's original method, and extensions and corrections have been proposed.45-47

Here, we will apply the extensions proposed by Louwerse et al.45 This approach includes solvent-specific effects and extensions derived from thermodynamic effects that were shown to improve solubility predictions for their set of test molecules, which included small molecules with a variety of different functional groups. In addition, the method splits the hydrogen bonding parameter into hydrogen bond donor and acceptor parameters. This allows the model to predict a negative enthalpy of mixing when one material is a strong hydrogen bond donor and the other is a strong acceptor, which is observed experimentally but is not predicted by the original HSP method. The Louwerse et al. extensions replace eq 1 with

$$d = 4(\delta D_1 - \delta D_2)^2 + (\delta P_1 - \delta P_2)^2 + (\delta H_{D_1} - \delta H_{D_2})$$
$$(\delta H_{A_1} - \delta H_{A_2})$$
(2)

where d is the parameter distance, δH_A is the hydrogen bond acceptor solubility parameter, and δH_D is the hydrogen bond donor solubility parameter. In this extension, the hydrogen bonding contribution to the cohesive energy density is $\delta H_A \times$ δH_D instead of δH^2 in Hansen's original method. If these values need to be compared, the split (acceptor and donor) hydrogen bonding solubility parameters can be converted to the original Hansen hydrogen bonding solubility parameter by taking the square root of their product, $\delta H_A \times \delta H_D$.

The distance in eq 2 is the square of the comparable Hansen distance in eq 1. This change is required for the addition of solvent-specific corrections. Additionally, the enthalpy of mixing has been shown to be proportional to d, not Ray which further supports the description in eq 2. To use the HSP method with the Louwerse et al. extensions, an effective radius (i.e., solubility cutoff distance), ref, must also be calculated for each solvent data point, to account for specific solvent and concentration effects

$$r_{\text{eff}} = \frac{x \ln(x) + (1 - x) \ln(1 - x)}{4 \ln(0.5) x (1 - x)} \left(\frac{1}{r_{\text{solute}}} + \frac{1}{r_{\text{solvent}}} \right)^{-1} - \frac{c_{\text{melt}}}{1 - x}$$
(3)

where x is the mole fraction of the solute, c_{melt} is an additional parameter that is fit to the data and represents a temperaturedependent value to account for the energy contained in the crystal structure of the solute, and r_{solute} and r_{solvent} are the solute and solvent radii, respectively. As in the original Hansen method, if the distance, d, is less than the radius, r_{eff} , the material is predicted to be soluble. Since r_{eff} is different for every solvent, and the new distance equation is not analogous to a distance in 3-D space, the sphere analogy used previously no longer applies; however, the cutoff distance for determining solubility has still been referred to as the effective radius.

The most straightforward way to experimentally determine the HSP value of a solute is to measure solute solubility in many different solvents and then fit the HSP value to the results of those experiments. 49,50 In the original Hansen method, with three parameters and no solvent-specific effects, this approach is equivalent to plotting the HSP values of good solvents in 3-D space and fitting a sphere around them to exclude the bad solvent HSP values. The extensions used

Membrane components Probe molecules TEMPO Poly(2,6-dimethyl-1,4-phenylene oxide) Naphthalene SO₃ Li SO₃-Li⁺ \$0°11 Ferrocene Phenoxyaniline trisulfonate, lithium counter-ion form Carboxaldehyde 4-Hydroxy-TEMPO Anthraquinone Li-POATS

Figure 1. Chemical structures of membrane components (left) and probe molecules (right) used in permeation experiments and analysis.

herein break this analogy, but the overall analysis process remains similar in principle.

A modification to this method, adopted in this study, is the inclusion of solvent mixtures in the solubility tests.⁵¹ The Hansen solubility parameter of a solvent mixture is equal to the volume-weighted average of the Hansen solubility parameters of the pure solvents.45 Including these points in the measurement allows the transition point from soluble to not soluble to be found with increased precision by having more data points and data points that are closer to the solubility limit.

MATERIALS AND METHODS

This study considers a cation-exchange membrane (POATS-PPO) prepared via functionalization of a poly(2,6-dimethyl-1,4-phenylene oxide) (PPO) backbone with a sulfonate group-containing side chain (phenoxyaniline trisulfonate or POATS). An illustration of the structure of the components of the membrane can be found on the left side of Figure 1, and the synthesis and processing of the membranes were described previously. 35 The polymer in this work is 7.2% substituted, i.e., 7.2% of the PPO repeat units had a POATS molecule substituted onto one of the methyl groups. This degree of substitution was chosen as it achieved a relatively high degree of substitution but not so high as to result in the loss of mechanical strength, which was observed for higher degrees of substitution. A 7.2% substitution corresponds to 20 wt % POATS in the membranes or an ion-exchange capacity of 1.44 mequiv g-1. Membranes with this degree of substitution have a measured solvent uptake of 32 wt % in dimethyl carbonate (DMC), which was the solvent used for all permeability measurements. This membrane and solvent system was chosen because the possible influence of the thermodynamic interactions was previously observed in this material, and the membrane was previously shown to not swell excessively or degrade over time in the chosen solvent and electrolyte.35

Six probe molecules were considered; the chemical structures of these molecules are shown on the right of Figure 1. These molecules were chosen from three common classes of redox-active materials: 9, metallocenes, aromatic organic compounds, and nonaromatic organic compounds. Within each category, two molecules were selected with different functional groups that were expected to give significantly different HSP values and to facilitate probing changes in interactions with the polymer backbone. The molecules were not necessarily chosen as the most desirable for energy-storage applications but as examples of the particular class of redox molecules and with functional groups expected to change measured HSP values. The chosen redoxactive metallocenes were ferrocene and a derivative molecule, ferrocene carboxaldehyde. The two nonaromatic organic redox-active materials were 2,2,6,6-tetramethylpiperidine-1-oxyl (TEMPO) and a derivative molecule, 4-hydroxy-TEMPO. Anthraquinone was selected

as an aromatic organic redox-active molecule, and while not used as a redox-active material, naphthalene was selected as the second aromatic organic molecule as a highly nonpolar molecule. Only the neutral forms of each molecule were considered to avoid introducing additional effects from ionic interactions.

Membrane Synthesis. Full synthesis and characterization of POATS-PPO were reported previously.35 In summary, POATS was synthesized via an aromatic sulfonation of phenoxyaniline. The procedure began by dissolving phenoxyaniline in 20% furning sulfuric acid in an ice bath, followed by slowly increasing the temperature to 80 °C. Triethylamine was then added, in an amount stoichiometrically equal to the theoretical number of sulfonate groups added to phenoxyaniline, to convert the product to the triethylammonium cation form. Then, calcium carbonate was added until the solution pH became neutral. Precipitated calcium sulfate was removed through filtration and drying, and the POATS product was purified by dissolving again in a small amount of water and repeating the filtration and drying process.

Brominated PPO (Br-PPO) was produced through the radical bromination of PPO using N-bromosuccinimide (NBS) and azobisisobutyronitrile (AIBN). All reactants were combined in a flask and dissolved in chlorobenzene at room temperature and subsequently heated to 110 °C in an oil bath. The reaction continued at 110 °C for 1 h. The reaction mixture was cooled, precipitated in reagent alcohol, and then collected by filtration. An additional round of purification was performed by dissolving the product in chloroform and precipitating in reagent alcohol again.

POATS-PPO was made by mixing a solution of Br-PPO in chlorobenzene with a solution of POATS dissolved in N-methyl-2pyrrolidone (NMP) together in a flask that also contained K2CO3 to neutralize the acid produced and NaI as a catalyst. This flask was heated in a 70 °C oil bath under a flow of nitrogen for 1 h. The polymer was precipitated using reagent alcohol and collected via centrifugation, then washed with more reagent alcohol, and collected again by centrifugation. The polymer was dried under vacuum, dissolved in NMP, and cast in a circular mold. The NMP was removed first in a convection oven at 70 °C followed by drying under vacuum at 70 °C, and the membranes were ion-exchanged to the lithium counter ion form by soaking the membranes in a 1 mol L-1 aqueous solution of LiCl for 24 h. Samples were rinsed in deionized water before use.

Solvent Uptake. Solvent uptake by the membrane was measured by first drying the membranes under vacuum for 24 h at 70 °C. The dry mass was then measured, and the membranes were placed in dimethyl carbonate (DMC). After 24 h, the solvated mass was measured after lightly wiping the surface to remove liquid drops. The membranes were placed back in DMC, and the solvated mass was measured again, 24 h later, to confirm that solvent uptake had plateaued. The membranes were then redried in a 70 °C oven at ambient pressure for 4 h followed by vacuum drying for a further 24 h,

and the dry mass was remeasured as well. Solvent uptake is reported as the percentage increase in mass from the dry to solvated state.

HSP Measurements. The HSP measurement procedure was developed and validated by measuring the HSP values of several molecules with previous literature reports. A comparison of the measured and literature values can be found in the Supporting Information, Section S1. The measurement procedure resulted in good agreement with literature values for uncharged materials, but a poor agreement was obtained for ionic compounds. The probe molecules tested in this work were thus limited to species that were

Hansen solubility parameters (HSPs) for each probe molecule and polymer component were measured experimentally, and a specific example is described in the Supporting Information, Section S2, with a flow chart in Figure S1. First, a concentration, in mg (solute) per mL (solvent), was chosen as a cutoff value for the solubility to make a distinction between a good or bad solvent. Typically, 20 mg mL-1 was used as an initial solubility concentration threshold. Solubility for a probe molecule was then determined by observing if the material being tested was soluble at that concentration in 10-12 solvents via visual inspection after stirring in each solvent for 24 h. The list of solvents that these were chosen from can be found in Table S2 along with their HSP values.

The measured HSP values had the best agreement with the literature reports when the material was considered soluble, according to the cutoff value, in 3-5 of the chosen solvents. When the concentration cutoff was too low, the predicted HSP values could change by a large amount when a new set of solvent data was added to the fit. With a higher concentration cutoff value, and more bad solvents than good solvents, the predicted HSP values were much less sensitive to the addition of new data. However, too high of a concentration made determining solubility more difficult since the solutions were typically colored and became darker at high concentrations and thus visual confirmation of the undissolved material was challenging under such conditions. Also, high concentrations limited the effectiveness of the solvent mixing step, described below, since any amount of poor solvent made the solute insoluble. Therefore, if fewer than 3 good solvents were found, the cutoff concentration was lowered, and the pure solvent solubility test was repeated. If the molecule was soluble in more than 5 solvents, the cutoff concentration was raised and the solubility test was repeated.

Once a concentration cutoff was chosen and good and bad solvents were identified, mixtures of the good and bad solvents were also evaluated for probe molecule solubility in five pairs of good and bad solvents, mixed together at different volume fractions in increments of 10%. Mixed solvent solubility experiments were performed until the volume ratio that caused the transition from soluble to insoluble at the cutoff concentration was found. A MATLAB program was then used to find the HSP value that resulted in the best agreement with the solubility data. Details on the algorithm used can be found in the Supporting Information, Section S3, and a flow chart of the process is provided in Figure S2.

Permeability Measurements. Probe molecule permeability was measured using a glass PermeGear Side-Bi-Side cell with 3.0 mL chambers separated by a POATS-PPO membrane with 0.317 cm2 of area exposed to the solution. An image of the experimental setup can be found in Figure S3. One chamber (donor side) was filled with a solution of a specific probe molecule in DMC, and the other chamber (receiving side) was filled with pure DMC. The probe molecule concentration on the donor side was 100 mM, except in two cases where there was a solubility limitation (anthraquinone, where a 5 mM concentration was used) or using 100 mM caused the receiving side concentration to exceed the measurable concentration range too quickly (naphthalene, where a 10 mM concentration was used).

The concentration of the receiving side solution was measured using ultraviolet-visible (UV-vis) spectrometry. Prior to the crossover experiment, a concentration vs absorbance calibration curve was measured for the probe molecule of interest. In all cases, the maximum receiving side solution concentration that could be measured was ~10% of the donor solution concentration. Over 4-

10 days, depending on the permeation rate, three concentration measurements were taken by removing solution from the receiving side, measuring absorbance at the calibrated wavelength, and returning the solution to the cell. The solution was typically removed from the receiver chamber for ~10 min for each concentration measurement, which was considered negligible when compared to the total experiment time of 4-10 days.

After the final measurement, the cell was disassembled, and the solvated membrane thickness was measured. The concentration vs time plot of these points was linear (all with $R^2 > 0.99$). The receiving chamber solution concentration vs time data was used to calculate the permeability as

$$\frac{-V_L L}{2 A} \ln \left(1 - 2 \frac{C_r[t]}{C_d[0]}\right) = Pt$$
(4)

where V_L is the liquid volume (3 mL), L is the membrane thickness in cm, A is the membrane area (0.317 cm^2) , C_d and C_r are the donor side and receiving side concentrations, respectively, in mM, and P is the permeability in cm2/s.

RESULTS AND DISCUSSION

Table 1 reports the measured HSP values for the membrane components and probe molecules. For each pair of probe

Table 1. Measured Dispersion (δD), Polar (δP), and Hydrogen Bonding (δH) Hansen Solubility Parameter Components for the Compounds in Figure 1a

compound	$\delta \mathrm{D}$	δP	$\delta H \left(H_D/H_A \right)$
PPO	17.6	3.4	2.3 (2.9/1.9)
POATS	17.2	14.7	19.5 (11.7/32.3)
naphthalene	17.7	2.7	5.8 (8.1/4.1)
anthraquinone	22.1	6.7	6.3 (5.1/7.8)
ferrocene	15.6	3.6	7.3 (4.7/11.3)
ferrocene carboxaldehyde	13.1	11.8	14.3 (10.2/19.9)
TEMPO	18.0	9.5	11.2 (8.9/14)
4-hydroxy-TEMPO	16.0	9.0	14.0 (13.3/14.8)

^aThe hydrogen bonding component is further split into hydrogen bond donor (HD) and hydrogen bond acceptor (HA) components.

molecules, the more polar version had slightly higher polar and hydrogen bonding components than the less polar molecule, as expected. Both PPO and naphthalene have HSP values reported in the literature, which match the measured values reasonably well (see Table S1). Of the compounds considered, POATS had the highest δP and δH values, which was expected as it was the only ionic molecule considered. Note that the previously discussed ionic molecule limitations of our HSP measurement and analysis procedure suggest caution in interpreting or comparing the POATS HSP value.

Measured probe molecule permeabilities through POATS-PPO are shown in Figure 2. In all cases, the more polar molecule in each category had a smaller permeability than the nonpolar molecule. This observation was consistent with the previous results, suggesting that more hydrophobic molecules may preferentially permeate through the hydrophobic regions of the polymer,35 and it could indicate that more polar or hydrophilic molecules interact less strongly with the membrane overall, partition less into the membrane, and thus contribute to a lower permeability compared to less polar molecules. The thermodynamic basis for this effect will be investigated in more depth in the following HSP analysis.

Before investigating the thermodynamic effects, it is important to recognize the potential contribution of probe

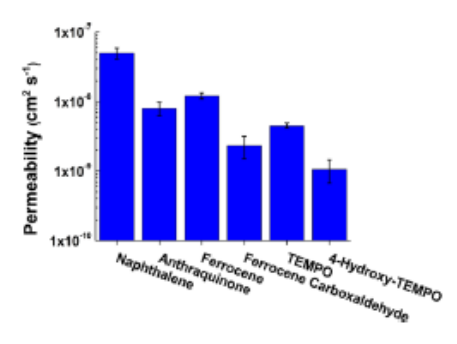


Figure 2. Permeability of probe molecules through DMC-solvated POATS-PPO membranes at room temperature. The results are reported as the average of three trials, and error bars represent one standard deviation from the mean.

molecule size effects to the observed permeability properties. Within this selection of probe molecules, the more polar molecule was always larger than the less polar version. Therefore, the observation that permeability decreased when molecule polarity increased (within a given pair, e.g., TEMPO to 4-Hydroxy-TEMPO) could be due in part to an increase in molecule size, which can affect the diffusion coefficient, and by extension the permeability. ^{25,53} To account for this size difference, a molar volume-based size correction factor for permeability was investigated (discussion of this analysis can be found in the Supporting Information, Section S4). Molecule size did not appear to impact the conclusions drawn from the permeability results because the probe molecules were all relatively similar in size. As such, the observed differences in permeability in Figure 2 appear to be much larger than differences in diffusion coefficients, due to molecule size, would explain. This analysis suggested that, at least for this selection of probe molecules, thermodynamic differences between the molecules may more significantly affect permeation properties compared to molecule size effects.

Permeability is proportional to a thermodynamic partition (or sorption) coefficient²⁵ that describes the solubility of the probe molecule in the polymer. Therefore, permeability is expected to be suppressed for probe molecules that have more unfavorable interactions with the membrane polymer because those molecules are not as soluble in the membrane as their counterparts that have more favorable interactions with the membrane. The HSP approach provides insight into the strength of these interactions via the parameter distance, defined in eq 2, involving the HSP values for the probe molecule and the membrane. A smaller distance is indicative of a smaller excess enthalpy or the situation where the probe molecule was likely more soluble in the polymer and thus more permeable. In other words, a negative correlation between HSP distance and permeability was expected for a series of probe molecules and a given polymer.

The HSP values for PPO and POATS were quite different, however, which was consistent with the chemical differences between the two compounds. For this reason, the distances between the probe molecules and the components of the membrane were calculated both separately and combined as detailed below. The combined value was calculated using a volume-weighted average of the components, which was the same method used for the solvent mixtures. The densities of POATS and PPO were assumed to be similar, and therefore the mass fraction was the same as the volume fraction.

The three approaches to analyzing the distance between the probe molecule and the membrane or polymer component are shown in Figure 3. Probe molecule permeability is plotted vs

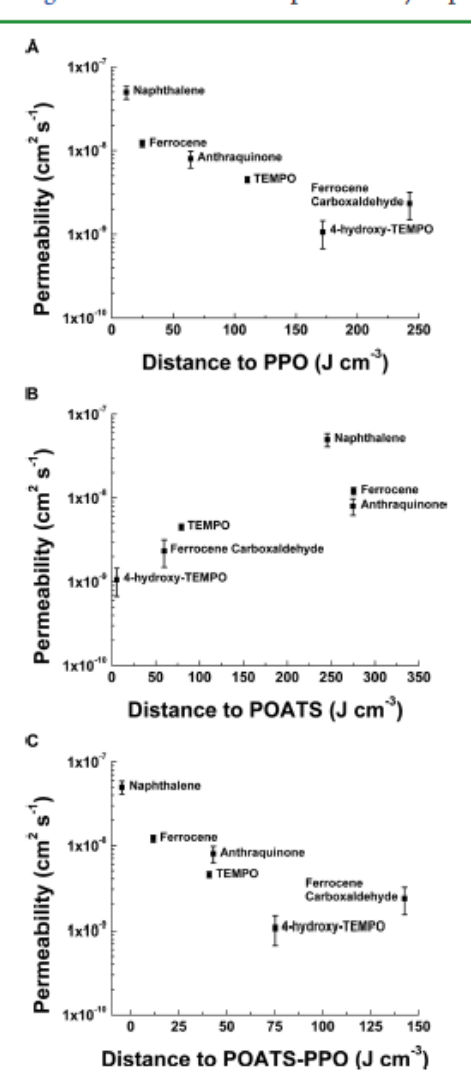


Figure 3. Permeability of probe molecules through POATS-PPO as a function of the HSP distance, which has units of energy density, between the probe molecule and (A) PPO, (B) POATS, and (C) POATS-PPO. The HSP value for POATS-PPO was taken to be the volume fraction weighted average of the HSP values of its constituents. The permeability results are reported as the average of three trials, and error bars represent one standard deviation from the mean.

the distance between (a) the probe molecule and PPO, (b) the probe molecule and POATS, and (c) the probe molecule and the combined POATS-PPO polymer. Figure 3A,C both exhibit negative correlations, and this situation was consistent with the physical picture, described previously, that permeability was expected to decrease as interactions between the probe molecule and the membrane component become less favorable. Alternatively, Figure 3B shows a positive correlation, suggesting that permeability was suppressed even though interactions between the probe molecule and POATS were more favorable.

The POATS-PPO membrane contains 80% PPO by mass, which likely led to the similarity of the trends in Figure 3A,C. Figure 3B appears to have the weakest correlation of the three,

which may be because the POATS side chain was only 20% of the membrane by mass and therefore that the contribution of the POATS interactions to permeability was less significant than the PPO interactions. The effect of probe molecule/ polymer interactions on permeability appeared to be dominated by interactions between the probe molecule and PPO backbone (Figure 3A,C); thus, the trend in Figure 3B may result not from interactions with the minority component POATS and the probe molecule but rather as a consequence of the differences in the HSP values of the PPO backbone and the POATS side chain. These results suggested that interactions between the probe molecules investigated here and the PPO backbone likely were more predictive of permeability and further suggested that transport of these probe molecules may predominantly occur in the hydrophobic PPO-rich regions of the membrane.

The suggestion that probe molecule permeability correlates strongest with interactions between the probe molecules and the hydrophobic PPO polymer backbone is different from observations in aqueous systems and suggests a potential key difference in the transport properties of membrane separators for nonaqueous vs aqueous flow battery systems. In aqueous systems, water, ions, and dissolved materials are generally ionic and/or polar, so these molecules likely interact primarily with polar, hydrophilic, regions of the polymer. If both the ions and redox molecules interact with the same part of the polymer in aqueous applications, it is reasonable that their transport, i.e., ionic conductivity and redox molecule permeability, is coupled and increased conductivity often comes with the expense of increased permeability (or crossover). In the same part of the polymer in aqueous applications, it is reasonable that their transport, i.e., ionic conductivity and redox molecule permeability, is coupled and increased conductivity often comes with the expense of increased permeability (or crossover).

This work suggests that membranes in nonaqueous systems may be fundamentally different. For example, in our previous work, increasing the charge density (i.e., POATS content) caused an increase in ionic conductivity and solvent uptake in POATS-PPO but essentially no change in ferrocene permeability.35 The HSP analysis here provides a potential explanation; ferrocene permeability was primarily dictated by interactions with the PPO backbone and not the POATS side chain. Therefore, ferrocene permeability was not appreciably affected by the relatively small changes in PPO content that occurred as the charge density (POATS content) of the material increased.35 These results, supported by the HSP analysis reported here, suggest an important decoupling of ionic conduction and organic redox molecule permeability that may inherently occur in nonaqueous RFB systems. Such decoupling would have advantages in membrane design because the hydrophobic polymer components could, in principle, be designed separately from the ionic polymer components. This approach could mitigate the often observed tradeoff relationship where conductivity often suffers as permeability/cross-over is suppressed.

Overall, while this study found a good correlation between the permeability and HSP-determined favorability of mixing, it is possible that other factors may affect permeability properties. This study considered only one membrane and one solvent, so different polymers or solvent systems may lead to different results. While the contribution of the solvent to the HSP analysis appears to not affect significantly the results of this study (as discussed subsequently), it is possible that specific interactions between some solvents and specific redox-active molecules could be important for describing cross-over properties. Furthermore, all probe molecules in this study

were uncharged and similar in size, and dramatic size differences or ionic charge could introduce additional complexity. In practice, varying fractions of the redox-active molecules will necessarily have a net charge when the battery is in operation. The charged nature of these molecules will add additional complexity potentially due to charge exclusion effects and/or changes in interactions that likely cannot be described using the HSP approach herein. The addition of ionic charge will also cause the HSP value of the redox material to change, and the HSP may also be affected by the counterions form it is in. As such, more research is needed to generalize this HSP approach, particularly with regard to the relative importance of the interactions investigated here compared to the effects of charge exclusion.

Additional material properties and interactions other than the polymer/solute interactions could be important to expand this analysis to consider different solvents and/or membranes. The interactions between the solute and solvent were investigated in Supporting Information, Section S5, but including them in the analysis resulted in a weaker correlation between permeability and HSP distances. Altogether, the combined permeability and HSP analysis suggested that solute interactions with the polymer backbone dominated over interactions between the solute and the solvent. The interactions between the polymer and solvent are also important, since the extent of membrane swelling strongly affects permeability and can affect membrane stability over time. These interactions between the solvent and the polymer, as well as the membrane solvent uptake, were not investigated as only one polymer and one solvent were considered. These interactions would likely need to be included in studies that compare different solvents, which could be an important additional step toward understanding specific solvent effects in membranes.

CONCLUSIONS

Thermodynamic interactions between redox-active molecules (or other organic solutes) and polymer membrane separators may be important for nonaqueous RFBs. A method was reported, using Hansen solubility parameters, to quantify these thermodynamic interactions and to investigate how they impact permeability or cross-over properties. The permeability of probe molecules through a membrane material correlated well with the solubility parameter distance between the probe molecules and the polymer backbone. This result suggested that thermodynamic effects have an important influence on permeability through the membrane, and solubility parameters could be useful in engineering membranes to minimize cross-over in flow battery systems.

These results also suggest that, unlike aqueous systems, nonpolar interactions are an important factor to consider in a nonaqueous RFB membrane separator. It was found that the organic probe molecules tested here were heavily influenced by interactions with the polymer backbone and less so with the charged side chain. Ionic conduction is generally most sensitive to the nature and concentration of charged groups in both aqueous and nonaqueous systems, but in aqueous systems, the ions and the redox-active materials likely interact with and transport through the same regions of the membrane separator. This study suggests a fundamentally different situation in nonaqueous systems where ions still preferentially interact with and transport through charge group-rich regions of the polymer but organic redox-active molecules preferentially

interact with and transport through backbone-rich regions of the polymer. Therefore, the transport of ions and redox-active molecules in nonaqueous membrane separators may be uniquely decoupled. This apparent decoupling represents an interesting opportunity for RFB membrane separator design because the hydrophobic polymer components could, in principle, be designed separately from the ionic (charged) polymer components to access unique and favorable combinations of ionic conductivity and redox-active molecule cross-over properties.

ASSOCIATED CONTENT

Supporting Information

The Supporting Information is available free of charge at https://pubs.acs.org/doi/10.1021/acsami.1c14845.

Additional experimental details including HSP measurement method validation, an example HSP measurement procedure, details on the HSP fitting algorithm, the effects of molar volume corrections on permeability, and the effects of including solvent data in the permeability/HSP distance correlation (PDF)

AUTHOR INFORMATION

Corresponding Authors

Gary M. Koenig, Jr. – Department of Chemical Engineering, University of Virginia, Charlottesville, Virginia 22904, United States; Phone: +1 (434) 982-2714; Email: gary.koenig@ virginia.edu; Fax: +1 (434) 982-2658

Geoffrey M. Geise — Department of Chemical Engineering, University of Virginia, Charlottesville, Virginia 22904, United States; Occid.org/0000-0002-5439-272X; Phone: +1 (434) 924-6248; Email: geise@virginia.edu; Fax: +1 (434) 982-2658

Author

Patrick M. McCormack — Department of Chemical Engineering, University of Virginia, Charlottesville, Virginia 22904, United States

Complete contact information is available at: https://pubs.acs.org/10.1021/acsami.1c14845

Notes

The authors declare no competing financial interest.

ACKNOWLEDGMENTS

This research was funded by the National Science Foundation, through Award IIP-1940915.

REFERENCES

- Weber, A. Z.; Mench, M. M.; Meyers, J. P.; Ross, P. N.; Gostick, J. T.; Liu, Q. Redox Flow Batteries: A Review. J. Appl. Electrochem. 2011, 41, 1137–1164.
- (2) Wang, W.; Luo, Q.; Li, B.; Wei, X.; Li, L.; Yang, Z. Recent Progress in Redox Flow Battery Research and Development. Adv. Funct. Mater. 2013, 23, 970–986.
- (3) Perry, M. L.; Weber, A. Z. Advanced Redox-Flow Batteries: A Perspective. J. Electrochem. Soc. 2016, 163, A5064—A5067.
- (4) Winsberg, J.; Hagemann, T.; Janoschka, T.; Hager, M. D.; Schubert, U. S. Redox-Flow Batteries: From Metals to Organic Redox-Active Materials. *Angew. Chem., Int. Ed.* **2017**, *56*, 686–711.
- (5) Sánchez-Díez, E.; Ventosa, E.; Guarnieri, M.; Trovò, A.; Flox, C.; Marcilla, R.; Soavi, F.; Mazur, P.; Aranzabe, E.; Ferret, R. Redox Flow

- Batteries: Status and Perspective towards Sustainable Stationary Energy Storage. J. Power Sources 2021, 481, No. 228804.
- (6) Qi, Z.; Koenig, G. M. Review Article: Flow Battery Systems with Solid Electroactive Materials. J. Vac. Sci. Technol. B 2017, 35, No. 040801.
- (7) Ha, S.; Gallagher, K. G. Estimating the System Price of Redox Flow Batteries for Grid Storage. J. Power Sources 2015, 296, 122–132.
- (8) Alotto, P.; Guamieri, M.; Moro, F. Redox Flow Batteries for the Storage of Renewable Energy: A Review. Renewable Sustainable Energy Rev. 2014, 29, 325–335.
- (9) Wei, X.; Pan, W.; Duan, W.; Hollas, A.; Yang, Z.; Li, B.; Nie, Z.; Liu, J.; Reed, D.; Wang, W.; Sprenkle, V. Materials and Systems for Organic Redox Flow Batteries: Status and Challenges. ACS Energy Lett. 2017, 2, 2187–2204.
- (10) Luo, J.; Hu, B.; Hu, M.; Zhao, Y.; Liu, T. L. Status and Prospects of Organic Redox Flow Batteries toward Sustainable Energy Storage. ACS Energy Lett. 2019, 4, 2220–2240.
- (11) Gong, K.; Fang, Q.; Gu, S.; Li, S. F. Y.; Yan, Y. Nonaqueous Redox-Flow Batteries: Organic Solvents, Supporting Electrolytes, and Redox Pairs. *Energy Environ. Sci.* **2015**, *8*, 3515–3530.
- (12) Cameron, J. M.; Holc, C.; Kibler, A. J.; Peake, C. L.; Walsh, D. A.; Newton, G. N.; Johnson, L. R. Molecular Redox Species for Next-Generation Batteries. *Chem. Soc. Rev.* 2021, 50, 5863–5883.
- (13) Shi, Y.; Eze, C.; Xiong, B.; He, W.; Zhang, H.; Lim, T. M.; Ukil, A.; Zhao, J. Recent Development of Membrane for Vanadium Redox Flow Battery Applications: A Review. *Appl. Energy* **2019**, 238, 202–224.
- (14) Wu, J.; Dai, Q.; Zhang, H.; Li, X. Recent Development in Composite Membranes for Flow Batteries. ChemSusChem 2020, 13, 3805-3819.
- (15) Machado, C. A.; Brown, G. O.; Yang, R.; Hopkins, T. E.; Pribyl, J. G.; Epps, T. H. Redox Flow Battery Membranes: Improving Battery Performance by Leveraging Structure—Property Relationships. ACS Energy Lett. 2021, 6, 158–176.
- (16) Yuan, J.; Pan, Z.; Jin, Y.; Qiu, Q.; Zhang, C.; et al. Membranes in Non-Aqueous Redox Flow Battery: A Review. J. Power Sources 2021, 500, No. 229983.
- (17) Xiong, P.; Zhang, L.; Chen, Y.; Peng, S.; Yu, G. A Chemistry and Microstructure Perspective on Ion-Conducting Membranes for Redox Flow Batteries. Angew. Chem., Int. Ed. 2021, DOI: 10.1002/ anie.202105619.
- (18) Uragami, T. Science and Technology of Separation Membranes, 1st ed.; Wiley, 2017.
- (19) Peng, S.; Zhang, L.; Zhang, C.; Ding, Y.; Guo, X.; He, G.; Yu, G. Gradient-Distributed Metal—Organic Framework—Based Porous Membranes for Nonaqueous Redox Flow Batteries. *Adv. Energy Mater.* **2018**, *8*, No. 1802533.
- (20) Montoto, E. C.; Nagarjuna, G.; Moore, J. S.; et al. Redox Active Polymers for Non-Aqueous Redox Flow Batteries: Validation of the Size-Exclusion Approach. J. Electrochem. Soc. 2017, 164, A1688— A1694.
- (21) Tung, S.; Fisher, S. L.; Kotov, N. A.; Thompson, L. T. Nanoporous Aramid Nanofibre Separators for Nonaqueous Redox Flow Batteries. *Nat. Commun.* **2018**, *9*, No. 4193.
- (22) Ok, B.; Na, W.; Kwon, T. H.; Kwon, Y. W.; Cho, S.; Hong, S. M.; Lee, A. S.; Lee, J. H.; Koo, C. M. Understanding the Enhanced Electrochemical Performance of TEMPO Derivatives in Non-Aqueous Lithium Ion Redox Flow Batteries. *J. Ind. Eng. Chem.* 2019, 80, 545–550.
- (23) Attanayake, N. H.; Kowalski, J. A.; Greco, K. V.; Casselman, M. D.; Milshtein, J. D.; Chapman, S. J.; Parkin, S. R.; Brushett, F. R.; Odom, S. A. Tailoring Two-Electron-Donating Phenothiazines to Enable High-Concentration Redox Electrolytes for Use in Nonaqueous Redox Flow Batteries. Chem. Mater. 2019, 31, 4353–4363.
- (24) Zhen, Y.; Zhang, C.; Yuan, J.; Zhao, Y.; Li, Y. Ferrocene/ Anthraquinone Based Bi-Redox Molecule for Symmetric Nonaqueous Redox Flow Battery. J. Power Sources 2020, 480, No. 229132.
- (25) Wijmans, J. G.; Baker, R. W. The Solution-Diffusion Model: A Review. J. Membr. Sci. 1995, 107, 1-21.

- (26) Baker, R. W. Membrane Technology and Applications, 3rd ed.; Wiley: New York, 2012.
- (27) Geise, G. M.; Paul, D. R.; Freeman, B. D. Fundamental Water and Salt Transport Properties of Polymeric Materials. *Prog. Polym. Sci.* 2014, 39, 1–42.
- (28) Donnan, F. G. The Theory of Membrane Equilibria. Chem. Rev. 1924, 1, 73–90.
- (29) Geise, G. M.; Lee, H.-S.; Miller, D. J.; Freeman, B. D.; McGrath, J. E.; Paul, D. R. Water Purification by Membranes: The Role of Polymer Science. J. Polym. Sci., Part B: Polym. Phys. 2010, 48, 1685–1718.
- (30) Geise, G. M. Why Polyamide Reverse-Osmosis Membranes Work so Well. Science 2021, 371, 31–32.
- (31) Mindemark, J.; Lacey, M. J.; Bowden, T.; Brandell, D. Beyond PEO—Alternative Host Materials for Li + -Conducting Solid Polymer Electrolytes. Prog. Polym. Sci. 2018, 81, 114—143.
- (32) Xue, Z.; He, D.; Xie, X. Poly(Ethylene Oxide)-Based Electrolytes for Lithium-Ion Batteries. J. Mater. Chem. A 2015, 3, 19218–19253.
- (33) Doyle, M.; Lewittes, M. E.; Roelofs, M. G.; Perusich, S. A.; Lowrey, R. E. Relationship between Ionic Conductivity of Perfluorinated Ionomeric Membranes and Nonaqueous Solvent Properties. J. Membr. Sci. 2001, 184, 257–273.
- (34) Doyle, M.; Lewittes, M. E.; Roelofs, M. G.; Perusich, S. A. Ionic Conductivity of Nonaqueous Solvent-Swollen Ionomer Membranes Based on Fluorosulfonate, Fluorocarboxylate, and Sulfonate Fixed Ion Groups. J. Phys. Chem. B 2001, 105, 9387–9394.
- (35) McCormack, P. M.; Luo, H.; Geise, G. M.; Koenig, G. M. Conductivity, Permeability, and Stability Properties of Chemically Tailored Poly(Phenylene Oxide) Membranes for Li+ Conductive Non-Aqueous Redox Flow Battery Separators. J. Power Sources 2020, 460, No. 228107.
- (36) Albergamo, V.; Blankert, B.; Cornelissen, E. R.; Hofs, B.; Knibbe, W. J.; van der Meer, W.; de Voogt, P. Removal of Polar Organic Micropollutants by Pilot-Scale Reverse Osmosis Drinking Water Treatment. Water Res. 2019, 148, 535–545.
- (37) Verliefde, A. R. D.; Comelissen, E. R.; Heijman, S. G. J.; Hoek, E. M. V.; Amy, G. L.; Van Der Bruggen, B.; Van Dijk, J. C. Influence of Solute-Membrane Affinity on Rejection of Uncharged Organic Solutes by Nanofiltration Membranes. *Environ. Sci. Technol.* 2009, 43, 2400–2406.
- (38) Barton, A. F. M. Solubility Parameters. Chem. Rev. 1975, 75, 731-753.
- (39) Saiz, C. A.; Darvishmanesh, S.; Buekenhoudt, A.; Van der Bruggen, B. Shortcut Applications of the Hansen Solubility Parameter for Organic Solvent Nanofiltration. J. Membr. Sci. 2018, 546, 120– 127.
- (40) Buekenhoudt, A.; Bisignano, F.; De Luca, G.; Vandezande, P.; Wouters, M.; Verhulst, K. Unravelling the Solvent Flux Behaviour of Ceramic Nanofiltration and Ultrafiltration Membranes. J. Membr. Sci. 2013, 439, 36–47.
- (41) Orme, C. J.; Stewart, F. F. Mixed Gas Hydrogen Sulfide Permeability and Separation Using Supported Polyphosphazene Membranes. J. Membr. Sci. 2005, 253, 243—249.
- (42) Ray, S. K.; Sawant, S. B.; Joshi, J. B.; Pangarkar, V. G. Development of New Synthetic Membranes for Separation of Benzene-Cyclohexane Mixtures by Pervaporation: A Solubility Parameter Approach. Ind. Eng. Chem. Res. 1997, 36, 5265–5276.
- (43) Hansen, C. M. The Three Dimensional Solubility Parameter and Solvent Diffusion Coefficient. Their Importance in Surface Coating Formulation; Danish Technical Press: Copenhagen, 1967.
- (44) Hansen, C. M. Hansen Solubility Parameters: A User's Handbook, 2nd ed.; CRC Press, 2007.
- (45) Louwerse, M. J.; Maldonado, A.; Rousseau, S.; Moreau-Masselon, C.; Roux, B.; Rothenberg, G. Revisiting Hansen Solubility Parameters by Including Thermodynamics. ChemPhysChem 2017, 18, 2999–3006.
- (46) Bustamante, P.; Peña, M. A.; Barra, J. The Modified Extended Hansen Method to Determine Partial Solubility Parameters of Drugs

- Containing a Single Hydrogen Bonding Group and Their Sodium Derivatives: Benzoic Acid/Na and Ibuprofen/Na. Int. J. Pharm. 2000, 194. 117–124.
- (47) Stefanis, E.; Panayiotou, C. A New Expanded Solubility Parameter Approach. Int. J. Pharm. 2012, 426, 29–43.
- (48) Hughes, J. M.; Aherne, D.; Coleman, J. N. Generalizing Solubility Parameter Theory to Apply to One- and Two-Dimensional Solutes and to Incorporate Dipolar Interactions. *J. Appl. Polym. Sci.* **2013**, *127*, 4483–4491.
- (49) Lin, X.; Jiang, G.; Wang, Y. Hansen Solubility Parameters of Coal Tar-Derived Typical PAHs Using Turbidimetric Titration and an Extended Hansen Approach. J. Chem. Eng. Data 2017, 62, 954– 960.
- (50) Liu, Y.; Zhang, B.; Kinsinger, C. L.; Yang, Y.; Seifert, S.; Yan, Y.; Mark Maupin, C.; Liberatore, M. W.; Herring, A. M. Anion Exchange Membranes Composed of a Poly(2,6-Dimethyl-1,4-Phenylene Oxide) Random Copolymer Functionalized with a Bulky Phosphonium Cation. J. Membr. Sci. 2016, 506, 50–59.
- (51) Milliman, H. W.; Boris, D.; Schiraldi, D. A. Experimental Determination of Hansen Solubility Parameters for Select POSS and Polymer Compounds as a Guide to POSS-Polymer Interaction Potentials. *Macromolecules* 2012, 45, 1931–1936.
- (52) Gupta, D.; Cai, C.; Koenig, G. M. Comparative Analysis of Chemical Redox between Redox Shuttles and a Lithium-Ion Cathode Material via Electrochemical Analysis of Redox Shuttle Conversion. J. Electrochem. Soc. 2021, 168, No. 050546.
- (53) Wilke, C. R.; Chang, P. Correlation of Diffusion Coefficients in Dilute Solutions. AIChE J. 1955, 1, 264–270.